Design and early performance of IGRINS (Immersion Grating Infrared Spectrometer)

Chan Park*[a], Daniel T. Jaffe[b], In-Soo Yuk[a], Moo-Young Chun[a], Soojong Pak[c], Kang-Min Kim[a], Michael Pavel[b], Hanshin Lee[d], Heeyoung Oh[a,e], Ueejeong Jeong[a], Chae Kyung Sim[c], Hye-In Lee[c], Huynh Anh Nguyen Le[c], Joseph Strubhar[d], Michael Gully-Santiago[b], Jae Sok Oh[a], Sang-Mok Cha[a], Bongkon Moon[a], Kwijong Park[a], Cynthia Brooks[b], Kyeongyeon Ko[a], Jeong-Yeol Han[a], Jakyoung Nah[a], Peter C. Hill[b], Sungho Lee[f], Stuart Barnes[g], Young Sam Yu[a], Kyle Kaplan[b], Gregory Mace[b], Hwihyun Kim[a], Jae-Joon Lee[a], Narae Hwang[a], Byeong-Gon Park[a,e]

[a]Korea Astronomy and Space Science Institute, 61-1 Hwaam-dong, Daejeon 305-348, South Korea; [b]Dept. of Astronomy, Univ. of Texas at Austin, 1 University Station, Austin, TX 78712, USA; [c]School of Space Research, Kyung Hee University, Yongin-si, Gyeonggi-do 446-701, Korea; [d]McDonald Observatory, Univ. of Texas at Austin, 1 University Station, Austin, TX 78712, USA; [e]University of Science and Technology, Daejeon 305-350, Korea; [f]Space Environment Laboratory, Seoul, Korea; [g]Stuart Barnes Optical Design, Amsterdam, Netherlands;

ABSTRACT

The Immersion Grating Infrared Spectrometer (IGRINS) is a compact high-resolution near-infrared cross-dispersed spectrograph whose primary disperser is a silicon immersion grating. IGRINS covers the entire portion of the wavelength range between 1.45 and 2.45μm that is accessible from the ground and does so in a single exposure with a resolving power of 40,000. Individual volume phase holographic (VPH) gratings serve as cross-dispersing elements for separate spectrograph arms covering the H and K bands. On the 2.7m Harlan J. Smith telescope at the McDonald Observatory, the slit size is 1″ x 15″ and the plate scale is 0.27″ pixel^{-1}. The spectrograph employs two 2048 x 2048 pixel Teledyne Scientific & Imaging HAWAII-2RG detectors with SIDECAR ASIC cryogenic controllers. The instrument includes four subsystems; a calibration unit, an input relay optics module, a slit-viewing camera, and nearly identical H and K spectrograph modules. The use of a silicon immersion grating and a compact white pupil design allows the spectrograph collimated beam size to be only 25mm, which permits a moderately sized (0.96m x 0.6m x 0.38m) rectangular cryostat to contain the entire spectrograph. The fabrication and assembly of the optical and mechanical components were completed in 2013. We describe the major design characteristics of the instrument including the system requirements and the technical strategy to meet them. We also present early performance test results obtained from the commissioning runs at the McDonald Observatory.

Keywords: spectrograph, immersion grating, high resolution, infrared optics, opto-mechanics, broad-band coverage

1. INTRODUCTION

Up to now, detector size and grating technology have limited the spectral grasp of high resolution spectrographs in the near-IR. At $R=\lambda/\Delta\lambda=40{,}000$, the H and K atmospheric windows together have about 20,000 independent spectral resolution elements but the windows are separated by a significant range of wavelengths where the atmosphere is opaque. Good sampling of both windows in the spatial and spectral directions with a long enough slit to permit point sources and accompanying sky to be observed simultaneously requires an array size of at least 2K x 2K. The length of a diffraction grating in waves determines the maximum possible spectral resolution. The number of illuminated grooves, however, determines the number of diffraction-limited resolution elements per order. Manufacturing limitations in the ruling process limit how coarse ruled gratings can be and therefore set a lower limit on the lengths of the orders. As a consequence of these combined limitations, high resolution spectrographs for the near-IR have not been able to deliver spectra with continuous coverage of large spectral bands.

*chanpark@kasi.re.kr; phone +82 42 865-2194

Ground-based and Airborne Instrumentation for Astronomy V, edited by Suzanne K. Ramsay, Ian S. McLean, Hideki Takami, Proc. of SPIE Vol. 9147, 91471D · © 2014 SPIE · CCC code: 0277-786X/14/$18 · doi: 10.1117/12.2056431

In order to profit from the sensitivity of modern IR detectors, infrared spectrographs must have all of their components at cryogenic temperatures. To maintain a high throughput, such instruments operating with natural seeing must have slit sizes comparable to the typical seeing image size. This angular scale is usually many times larger than the diffraction-limited angular resolution. To reach a given resolving power with a slit m times wider than the diffraction limited angular scale, a diffraction grating must be longer in the direction of incidence by the same factor of m. This requirement drives high-resolution spectrographs to large sizes, a fact that presents significant challenges in a cryogenic instrument.

Immersion gratings break the size-resolving power curve for spectrograph designs.[1,2,3,4] An immersion grating of a given size made from Si has the same resolving-power slit-width product as a front-surface grating that is 3.4 times larger. Use of immersion gratings can therefore reduce cryogenic instrument volumes by an order of magnitude or more for a given resolving power and slit size. Lithographically produced Si immersion gratings also make it possible to have instrument designs with continuous wavelength coverage at high resolving power.[5,6] The lithographic gratings have superbly blazed grooves that give them high efficiency in high order and the process permits coarse enough rulings to allow entire orders to fit onto a single detector.

IGRINS, the Immersion GRating INfrared Spectrometer, is a joint project of the Korea Astronomy and Space Science Institute and the University of Texas at Austin. It has a resolving power R=40,000 and covers all wavelengths between 1.4 and 2.5 microns where the atmosphere transmits with ~3.5 pixel sampling of the spectral resolution elements. The instrument has a fixed format and no moving parts within the spectrograph. We have previously described the basics of the instrument design.[7] In this paper, we provide more details about the design, describe the integration and test process, and present performance numbers and sample science results from our first two commissioning runs on the 2.7m Harlan J. Smith telescope at McDonald Observatory.

2. INSTRUMENT OVERVIEW

2.1 Optical design

The IGRINS optical system is designed to cover as large simultaneous wavelength range as possible while maintaining a spectral resolving power of 40,000. Fig. 1 shows the IGRINS optical design layout.

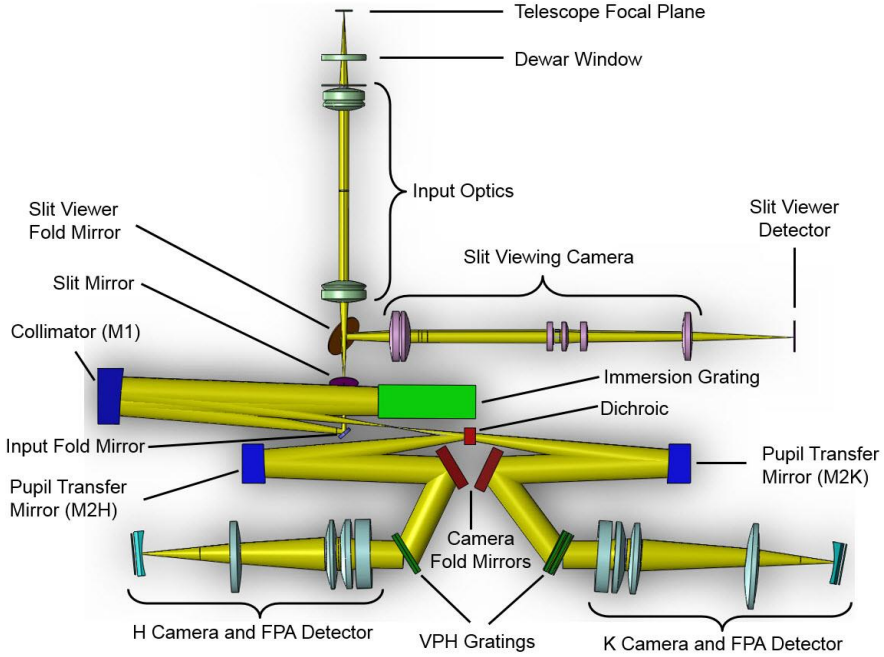

Figure 1. IGRINS optical design layout. Three of the four functional units are displayed: input relay optics, slit-viewing camera, and H-band and K-band spectrograph camera modules (calibration unit not shown).

IGRINS employs a white pupil optical configuration[8] where the pupil formed on the immersion echelle is reimaged onto a second pupil at the cross-disperser. The instrument consists of four functional units including a wavelength calibration (outside of the cryogenic system), pre-slit input relay optics, a slit monitoring and guiding imager, and H- and K-band spectrograph camera modules. Each camera includes its own detector system. There is no moving part inside the cryogenic system since the instrument already covers all available spectral range within its operating band. Unique features of IGRINS include the use of a silicon immersion echelle grating as the main disperser and volume phase holographic gratings as the cross-dispersers.[4,9]

The entire optical design contains total nineteen powered lenses and seven mirrors including three aspherical off-axis aluminum collimating mirrors and two toroidal Infrasil field flattening lenses. The telescope focus is external to the cryostat. A foreoptics assembly forms an image of the telescope primary on a cold baffle and then reimages to the slit plane. Light passing through the slit first strikes a fold mirror before reaching the primary collimator (M1 in Fig. 1). The collimated light proceeds to the immersion grating, and the collimator reflects the dispersed beam again to form a column of multicolored images of the dispersed slit. A dichroic just after this polychromatic focus splits the beam between the two spectrograph arms where the beams reach the H and K pupil transfer mirrors (M2 in Fig. 1). Each pupil transfer mirror collimates the beam once again and forms the second (white) pupil on a VPH grating. Collimated beams throughout the instrument have a diameter of 25 mm. In each spectrograph arm, the light from the cross-disperser enters a refractive camera that images the echellogram onto a 2048 x 2048 Teledyne HgCdTe array.

2.2 Mechanical and opto-mechanical design

Apart from the warm calibration system, all of IGRINS resides within a custom-designed cryostat. This highly compact vessel (longest dimension < 1 m, Fig. 2) consists of three components: top and bottom plates and a solid-body sidewall. The inner sides of the top and bottom plates have a supporting rib structure to help maintain flatness against 100 kPa atmospheric pressure when the system is under vacuum. For a rectangular Dewar, we need to control wall deformation to insure vacuum integrity.[10] The O-ring based sealing system maintains high vacuum of typically lower than 10^{-6} Torr. There is no mechanical interference when the top cover and the sidewall are removed, since all electrical, vacuum, and mechanical feedthoughs pass through the bottom plate. The 40 mm diameter and 5 mm thick ZnSe Dewar window deforms only at the sub-micron level (0.5 μm at its center). The window material discourages condensation even in a high humidity environment.[11] The mass of cryostat including all the internal components is about 200 kg.

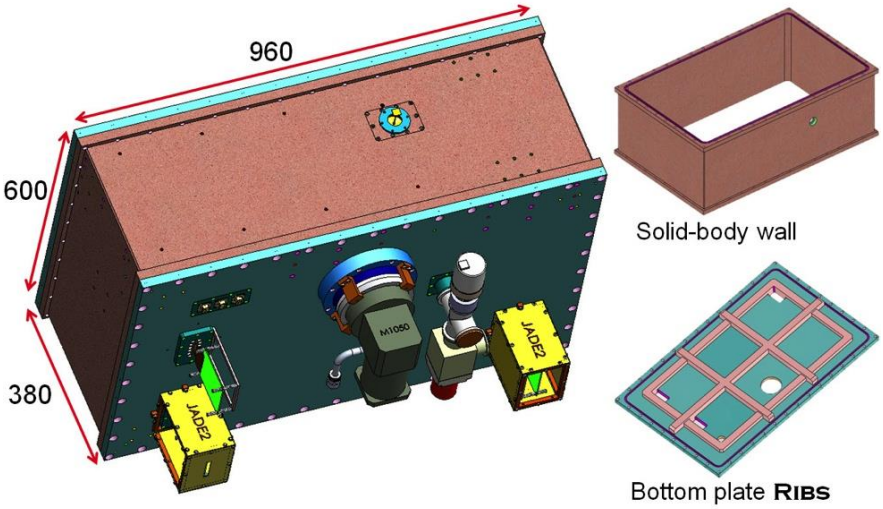

Figure 2. IGRINS cryostat 3D model. Dewar dimensions are given in millimeters.

The cryostat optical bench is an 880 x 520 mm rectangular plate. The bench accommodates all of the IGRINS optical components in a planar layout. Fig. 3 displays a CAD rendering of the optical bench with the components in place. The back side of the bench plate is partially cut-out to reduce the total cold mass while maintaining stiffness. The bench has a small indentation around its perimeter to provide a better light-tight fit for the radiation shield. The bench surface was fabricated with high precision (the measured flatness was 13 μm peak to valley). All the optical elements were positioned

by locating pins and pin holes. The optical compensators have their positions adjustable by using a set of bumpers and shoulder screws.[12,13]

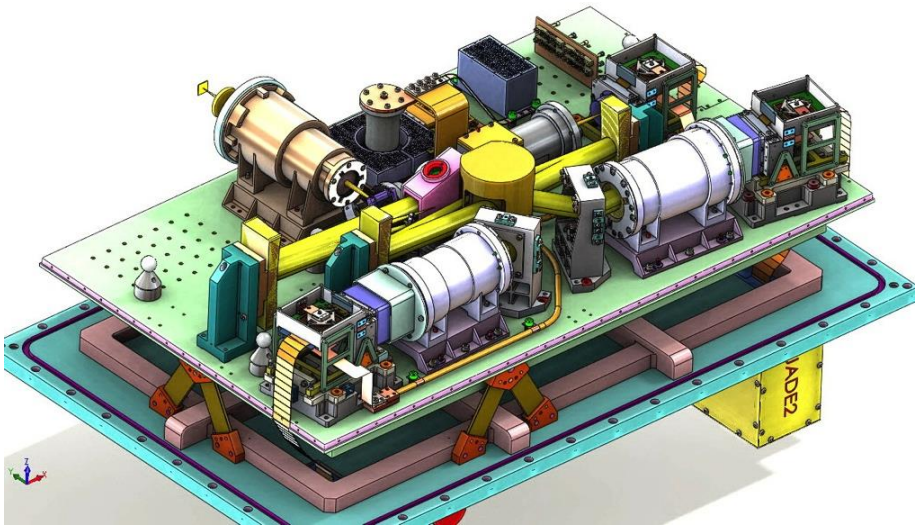

Figure 3. Optical bench and the components above it.

Gravitational flexure analysis says that normal operation can cause up to a 25 μm deflection on the K-band corner of the optical bench (Fig. 4). It may produce up to 5 μm of surface deflection of the bench in a one-hour exposure observation. This is consistent with the instrument flexure experiment during the first commissioning run meaning that the K-band wavelength shift is larger than the H-band (see section 4.3). Atmospheric pressure causes a 220 μm deflection at the center of bottom plate. The given stresses are well within the margins for cryostat structural safety. Structural analysis of the cryostat design tells us that it meets the system alignment and stability requirements. This theoretical analysis was confirmed by a variety of optical tests at different telescope orientations during test observations at McDonald Observatory in March and May 2014.

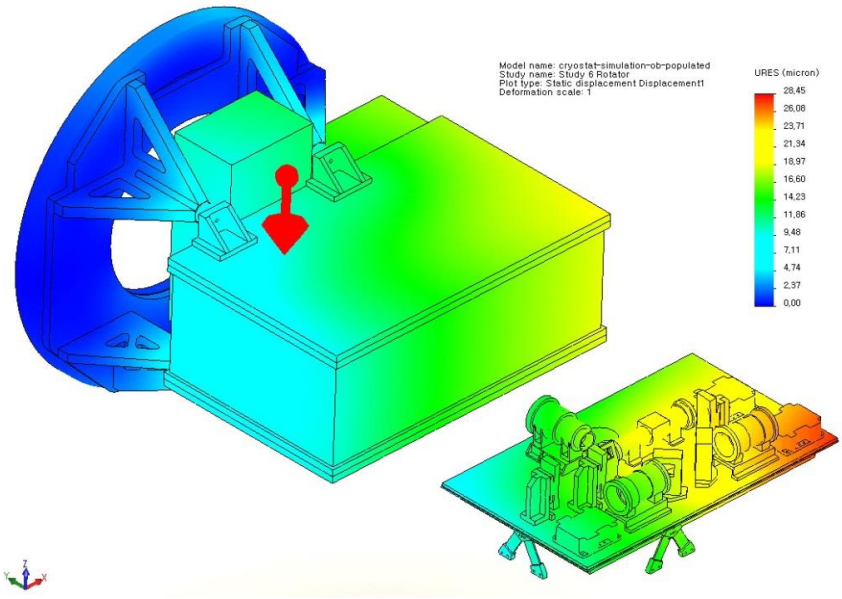

Figure 4. Structure analysis showing the stability of the IGRINS cryostat and optical bench. The maximum deflection occurs near the K-band detector but is small enough to meet the optical component stability tolerances. The color bar gives the scale of the deflection in micrometers.

The stability of each optical element has been numerically tested by the finite element method (FEM). Fig. 5 shows one example for the gravitational flexure of the M1 collimator.[13] The figure indicates the gravity vector orientation that produces the maximum deflection.

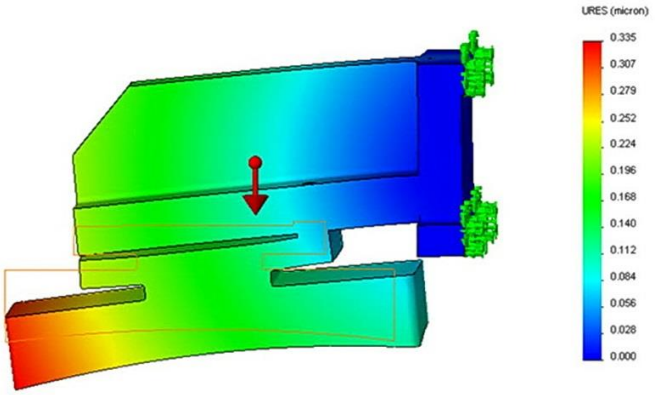

Figure 5. Displacement distribution of the M1 collimator caused by 1G gravity normal to the mirror surface. The largest geometric distortion is 0.30 μm and minimum distortin is 0.10 μm within the clear aperture, corresponding to 0.46″ tilt from the fiducial mirror surface.

2.3 Cryogenics

Thermal background photons in the H and K bands produced by the optical components and surrounding mount material need to be suppressed to below the detector's dark noise level, 0.01 electrons per second, as demanded by the top level science requirements. Based on this requirement, we set the operating temperature to 130 K for the optics and their mounts and to 65 K for the three detectors. Instead of liquid cryogens, we use a closed-cycled mechanical cooler, a CTI M-1050 two-stage refrigerator system. Numerical models of heat loads and flows through the system were performed before we finalized the cryogenic design. Figure 6 illustrates the theoretical temperature distribution of the optical bench, the radiation shield, and the optical components inside. All the cold mass remains between 125 K and 130 K with the temperature gradient smaller than 4 K per 100 mm. The gradient requirement assures us that the differential thermal contraction on the bench is smaller than the typical machining tolerance of 10 μm.

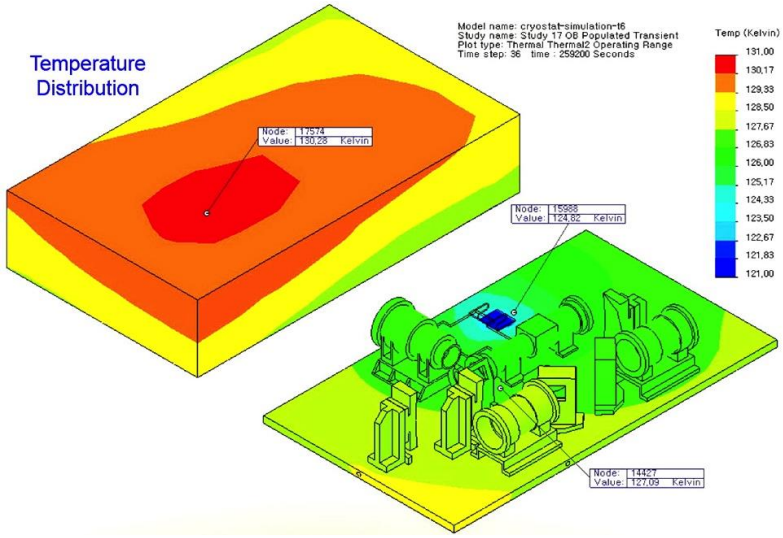

Figure 6. Cryogenic models. Temperature distribution of major cryogenic components is illustrated. All the components including the optical bench and the radiation shield remain between 125 K and 130 K with the gradient far smaller than 4 K per 100 mm everywhere.

Fig. 7 shows temperature versus time curves for the optical bench, the immersion grating, and the detectors. The as-built cryogenic performance of IGRINS closely matches the behavior predicted from the design. The instrument reaches its nominal operating temperature, 130 K for the immersion grating and other optical components and 65 K for three H2RG focal plane array detectors in 30 hours. If the immersion grating temperature changes, variations in the refractive index of silicon are sufficient to violate our top level requirements for wavelength stability. We therefore require the immersion grating temperature to remain within 60 mK of its reference temperature. Our lab experiment confirmed that this stability requirement is well met by an active thermal control mechanism. The optical bench and detector temperatures are also kept stable enough for their operation. To avoid any possible thermal shock, the detector substrates need to be cooled or warmed up slowly, < 0.5 K/min. The measured cooling rate is about 0.15 K/min as indicated on the graph. For the detailed design and thermal analysis of detector mount systems, Oh et al. (2014) described the procedure and results in a separate paper.[12]

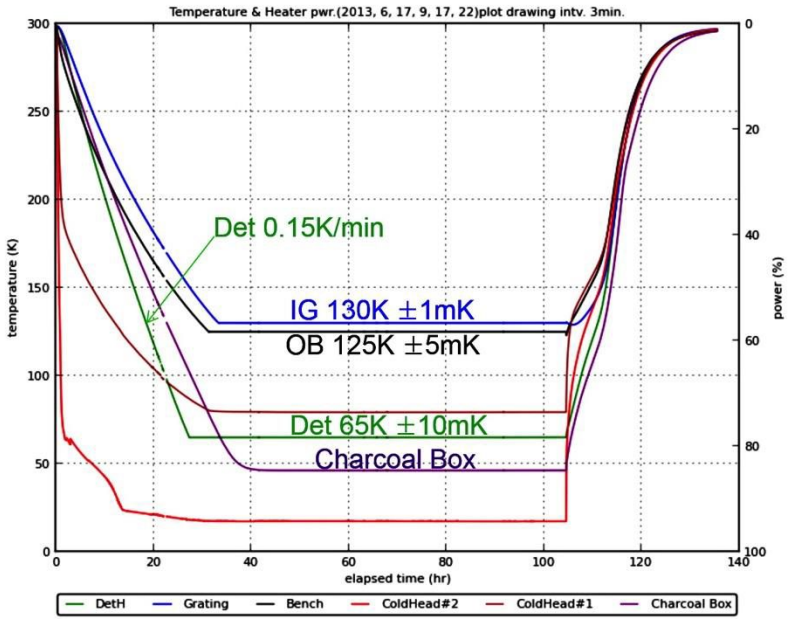

Figure 7. Cooldown and warm-up curves. The system cooling time to reach operating temperatures and warm-up time to reach room temperature are shown. Detector cooling rate and each component's temperature stability in operation are also marked in measured RMS values.

2.4 Electronics

IGRINS employs three Teledyne H2RG HgCdTe detectors. The H- and K-band spectrograph channels use science-grade 2.5 μm cutoff sensors, while the slit-viewing camera makes use of an engineering-grade sensor. Each detector set is controlled by a SIDECAR ASIC cryogenic board and a JADE2 USB interface card. We measured various characteristic properties of the detectors during the laboratory experiments including readout noise, system conversion gain, signal linearity response, dark current, reference-level stability, etc. The characterization and optimization of IGRINS detectors are separately reported elsewhere in these Proceedings.[14]

2.5 Software

The IGRINS software consists of six functional packages. Sensitivity estimates made with the Exposure Time Calculator (ETC) and a finding chart (both available within the Observational Preparation Package) can be useful in planning for and executing the observations. During the observation, Housekeeping Package, Slit Camera Package, Data Taking Package, and Quick Look Package software tools are designed to be conducting the observation. After the observation, the obtained data can be reduced by the Pipeline Package (PLP). This package can also be used during the observing night to help an observer to decide further observation strategies. The PLP performs the reduction of echellogram images with the following procedures: flat fielding, background removal, order extraction, distortion correction, wavelength calibration, and telluric correction. The echellogram mapping functions are straightforward enough to be theoretically

defined since the instrument has no moving part in it. More details of the IGRINS software are given in Sim et al. (2014).[15]

3. FIRST LIGHT

3.1 Optical alignment in the laboratory

Alignment of a complex cryogenic optical system with no cold adjustments presents some unique challenges. Tolerance analysis of the IGRINS design indicated that it would be possible to place most components on the cryostat optical bench using precision machining of the pin locations and then to make a minimum number of final adjustments to correctly place the echellograms on the spectrograph detectors and to optimize the image quality in the slit-viewing and spectrograph cameras. Prior to integrating the full system, we tested each of the four camera subsystems, the foreoptics, the slit-viewing camera optics, and the H and K spectrograph cameras in a separate test Dewar to confirm that the cryogenic performance of each subsystem at optical wavelengths was within tolerance. Since the primary on-axis deviation with temperature was a defocus, this test provided adequate assurance that the subsystems would perform well in the infrared. Within IGRINS, the available adjustments included the pitch, yaw, and focus of the detectors, tilt of the immersion echelle in two directions, and pitch of the VPH gratings in the dispersion direction alone. Each of these adjustments needs to be made with the system warm by changing out hard bumpers or shims. With some useful aids and a careful procedure, we were able to complete the alignment of IGRINS in a minimum number of cooldowns (5-7 times, depending on how you count).

Our first task was to align the slit-viewing camera. At the slit plane, we insert a lithographically patterned target plate (Fig. 8). The slit mirror is tilted 22.5° with respect to the slit plane, so this plate should only be in focus along the diagonal line (upper left to lower right in Fig. 8) where the slit lies. The relative focus along this line gives the deviation of the slit-viewing camera from the correct yaw while the image size variation in the perpendicular direction gives the detector focus. Once the slit-viewing camera is in focus, it can act as a proxy for the slit image.

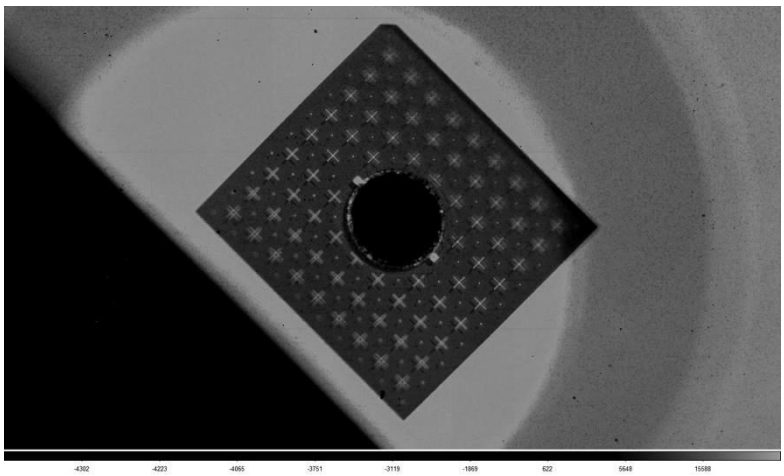

Figure 8. Image of the temporary target plate taken with the IGRINS slit-viewing camera. The slit would run from upper left to lower right at the position of the central hole. The plane of this plate is tipped with respect to the focal plane allowing the image sizes to be used to determine focus and yaw of the slit-viewing detector.

To focus the spectrograph cameras, we retain the target plate, which has a large central hole and place a pinhole at the external focus. With a ThAr lamp behind the pinhole, we can adjust the tip of the cross-dispersers to place the correct orders onto each spectrograph camera. The series of monochromatic images of the pinhole allow us to test the image quality over the entire echellogram. By moving the pinhole in the axial direction, we can then determine both the overall focus of each spectrograph camera and the tip and tilt necessary to get the best compromise orientation for image quality at all wavelengths. When we now place a hot source behind the pinhole, we can measure the power distribution along each order and tilt the immersion echelle to center the blaze on the detectors. Figure 9 illustrates the part of this procedure where we checked the optical performance with images of the external pinhole. The insets in the figure clearly show the image quality difference of before and after a detector focal adjustment procedure.

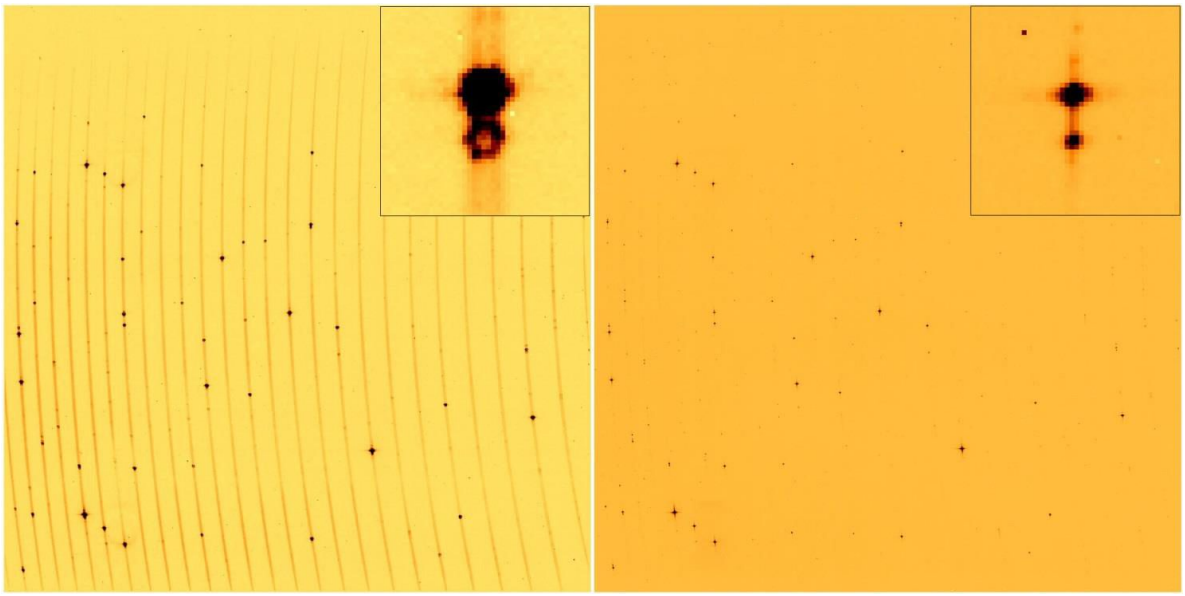

Figure 9. Spectrograph detector focal adjustment procedure. The insets distinctively illustrate the difference of image quality before and after a focus adjustment.

3.2 Commissioning runs

IGRINS has had two commissioning runs on the McDonald Observatory 2.7 m Harlan J Smith telescope in March and May of 2014. The purpose of these runs was to debug the system hardware and software, to measure the instrument performance and to provide a sample dataset for tests of the data reduction software and to facilitate planning of future astronomical observing programs. Figure 10 shows an image of the instrument mounted on the 2.7 m telescope. The black metal box between the cryostat and telescope rotator is the calibration unit. It consists of three linear moving stages, three mirrors, a beam combiner, a tungsten halogen lamp for flat, two hollow cathode lamps, and a 2-inch Infragold integrating sphere. The white aluminum frame is the electronics rack housing three detector computers, three LakeShore temperature controllers, a power supplier, and a network switch.

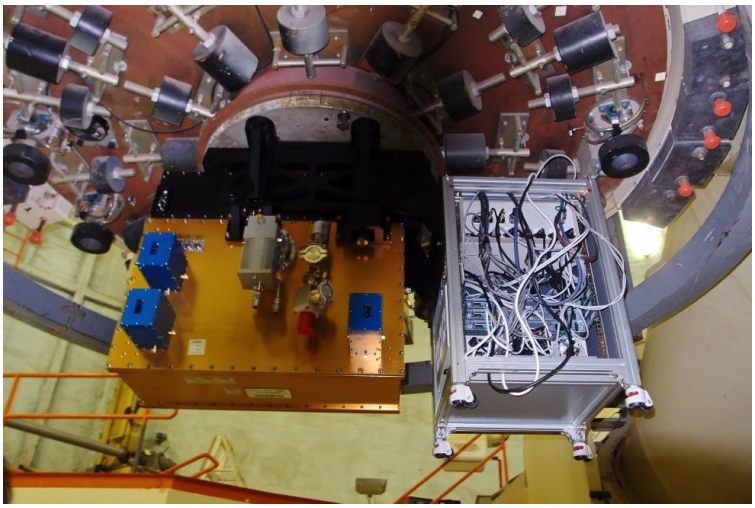

Figure 10. IGRINS on the 2.7m Harlan J Smith telescope at the University of Texas McDonald Observatory. The cryostat is the gold box on the left. The three protruding blue boxes contain the Teledyne JADE2 USB interface cards. The CTI cold head and vacuum pump fitting are at the center of the side facing the reader. To the right is the electronics rack which holds the three detector computers and other auxiliary hardware.

Target acquisition and guiding is always an issue in the infrared where interesting targets can be extremely faint at visible wavelengths or have a significantly different morphology. To insure the speed and reliability of target acquisition, IGRINS uses a direct slit-viewing camera that operates in the K band. A set of slit-viewing optics images the slit plane to an engineering grade 2048 x 2048 Teledyne 2.5 μm cutoff HgCdTe array. The total field of view of the camera is nearly 2′ x 3′ and the pixel scale is 0.12″ pixel^{-1}. Figure 11 shows a sample image from the camera, taken toward the center of the Orion nebular. In this image, the core of θ^1C Ori is saturated.

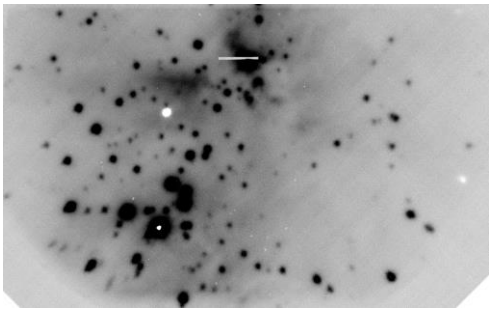

Figure 11. Part of an IGRINS slit-viewing camera image of the Orion molecular cloud. The main Trapezium stars are visible at the lower left and the slit lies partially in front of the Becklin-Neugebauer object.

One of the more interesting pieces of sample data is a spectrum taken toward the northwest lobe of the Orion-KL outflow. This spectrum consists of an ABBA sequence with the A position about 15″ northwest of the Becklin-Neugebauer object and the B, or "off-", position about 30″ to the east at a dark location in images of the H_2 v=1-0 S(1) line at 2.122 μm. The left panel of Fig. 12 shows a raw image of a slit A position where no sky background subtraction has been done. The image includes many sharp airglow lines, neutral hydrogen and helium emission lines (marked on the figure), too.

The right panel of Fig. 12 shows the On-Off spectra of several of the H_2 transitions in the Orion-KL outflow. The slit is 15″ long so the false-color image shows an east-west position velocity diagram along a cut through the outflow. Already from these images one can notice that the structure of the shock is enormously complex. Further observations will permit us to map intensity as a function of position and velocity and transition across the outflow.

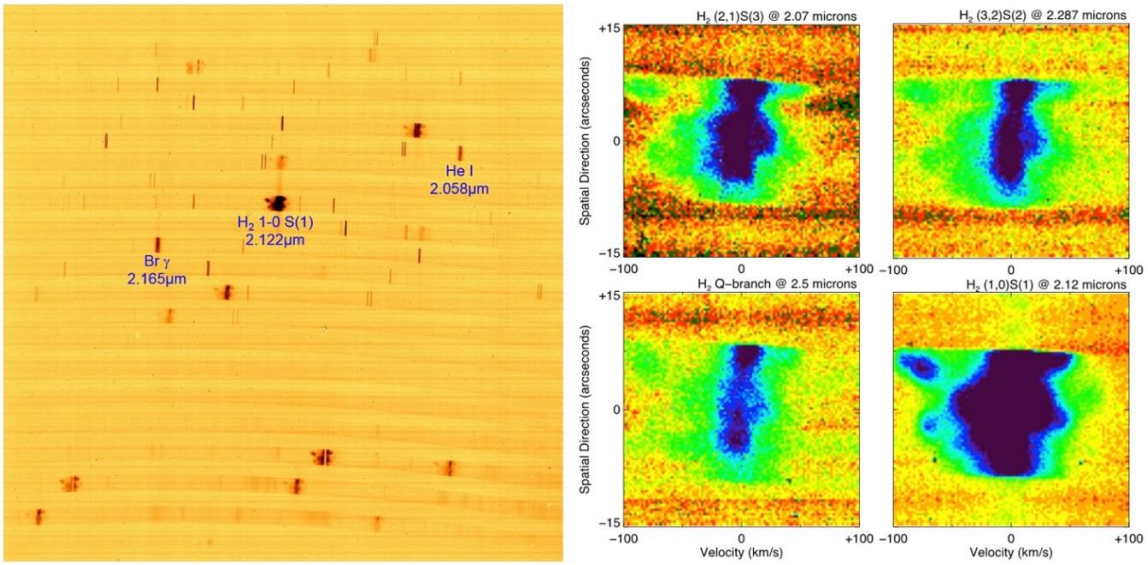

Figure 12. K-band spectroscopic sample data of the north-west lobe of the Orion-KL outflow. The left panel shows the K-band echellogram in which a few of the lines have been identified and labeled. The right panel shows false-color position velocity diagrams for a selection of lines from the echellogram on the left. The slit length is 15″ and each sub-panel covers 200 km s^{-1} in velocity.

4. INSTRUMENT PERFORMANCE

On the initial observing runs, we were able to measure the spectral resolving power, signal-to-noise ratio, and spectral stability driven by instrumental flexure.

4.1 Spectral resolution

IGRINS' design resolving power R is 40,000 throughout H and K bands. We used ThAr lines both to determine the instrumental dispersion and to measure the width of the spectral point spread function. Two identified ThAr lamp lines of 1.74500 μm and 1.73008 μm are located on a same row in a lamp echellogram, but their columns are separated 1282 pixels. This gives us a pixel scale of 1.164 x 10^{-5} μm/pixel. As shown in Fig. 13, the typical measurement of the FWHM of a singlet emission line is about 3.3 pixels. It provides the resolution element of 3.841 x 10^{-5} μm and the resultant resolving power of about 45,000. This is a naturally expected outcome since the installed actual IGRINS slit width is slightly narrower than the designed one.

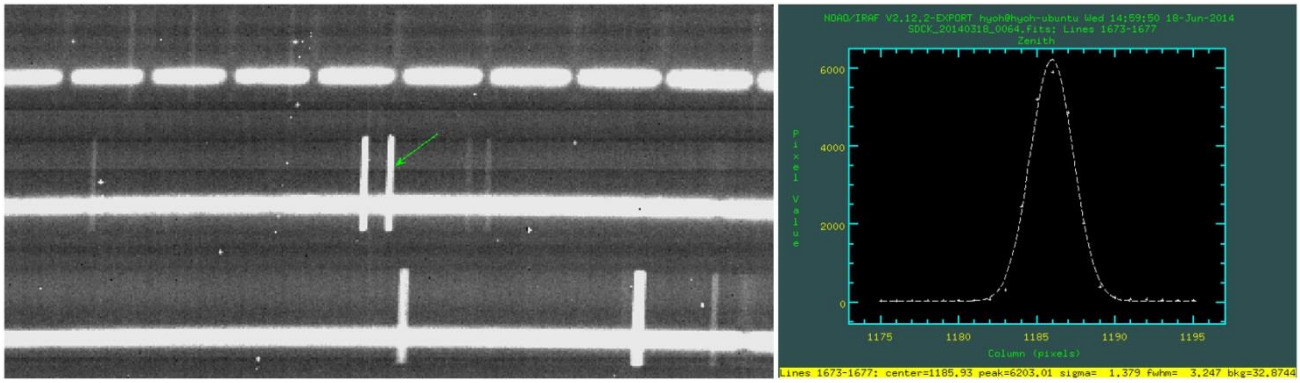

Figure 13. A section of observed echellogram of an A0V star (left) and a fitted profile of an airglow emission line (right).

4.2 Sensitivity

The IGRINS software development included an exposure time calculator. In the existing version of this calculator, we used throughput predictions based on the predicted or measured properties of the optics and factored in the nominal performance of the detectors. We have observed more than 60 sample objects with various exposure times during our two commissioning runs. The sample objects cover a broad range of spectral types, from B to M and the sample also includes highly embedded protostars. From these sample data we estimate the observed signal-to-noise ratios (SNR) and compare them with the predictions of our exposure time calculator. We used two different methods to estimate the signal to noise ratio per spectral resolution element: $SNR_1 = \sqrt{S_{dn} \cdot N \cdot g}$ and $SNR_2 = (S_{dn}/\sigma_{dn})\sqrt{N}$, where S_{dn} is the peak value on a stellar continuum near the central region of a K-band echellogram in ADU, g is the measured system conversion gain (2.21electrons per ADU)[14], σ_{dn} is the measured local root-mean-square (rms) value along the stellar continuum in ADU, and N is the number of pixels covered by the area of one resolution element at the wavelength where the S_{dn} is measured.

We calculated the SNR_1 and SNR_2 for 14 K-band observed spectra including five A-type stars, five M-type stars, one B star, one Ae/Be star, one G star, and one IR Class I object (Table 1). These two methods produce very consistent results within 5 % of the values. They did not show any particular spectral type dependence in our statistics. For only one case, the measured SNR showed below 50 % of the ETC calculated value, believed due to bad weather condition during the exposure. The other cases resulted in 83 % and 84 % of ETC values, on average, for SNR_1 and SNR_2, respectively.

Table 1. Comparison of ETC-predicted and measured SNR. FWHM and N are measured in pixel.

	Object	Exp.t[s]	Airmass	Kmag	spec. type	ETC	SNR_1	SNR_2	S_{dn}	σ_{dn}	FWHM	N
1	HD 34317	120	1.38	6.30	A0V	**193**	**136**	**173**	200	8	12	42
2	HD 89239	240	1.03	6.60	A0V	**238**	**272**	**254**	1200	25	8	28
3	HD 89239	300	1.05	6.60	A0V	**267**	**277**	**260**	1100	24	9	32
4	HD 95735	60	1.09	3.34	M2	**550**	**289**	**259**	900	23	12	42
5	HD 95735	20	1.08	3.34	M2	**317**	**106**	**96**	90	7	16	56
6	Serpens15	240	1.15	7.05	ClassI	**193**	**167**	**137**	600	20	6	21
7	HD179218	120	1.05	6.00	Ae/Be	**222**	**215**	**229**	1000	20	6	21
8	EK Dra	240	1.23	5.91	G1.5	**330**	**227**	**224**	700	18	9.5	33
9	GJ 581	150	1.35	5.84	M5	**268**	**204**	**192**	600	18	9	32
10	HIP 94620	120	1.08	5.30	A4V	**309**	**235**	**195**	950	25	7.5	26
11	P Cygni	60	1.03	3.27	B1	**558**	**265**	**322**	1300	20	7	25
12	HIP 66634	120	1.09	5.17	A3	**328**	**309**	**362**	1900	25	6.5	23
13	HD 95735	90	1.15	3.34	M2	**662**	**654**	**541**	8500	75	6.5	23
14	CM Dra	240	1.12	7.80	M4.5	**135**	**133**	**167**	350	10	6.5	23

4.3 Spectral stability

Radial velocity stability in a spectrograph begins with mechanical stability. Gravitational flexure of the instrument along the main dispersion direction will be the major cause of shifts in line positions. For IGRINS, a one-pixel shift translates to an RV change of 2 km/s. To estimate the possible instrumental flexure, we took a series of ThAr emission lamp spectra in the H and K bands while varying the orientation of the instrument. On the night of 2014 March 15, at the McDonald 2.7 m telescope, we measured calibration lamp images at 1,2, and 3 airmasses with the slit oriented both east-west and north-south. We reached each airmass by moving the telescope due south from the zenith. By extracting and cross-correlating the same row (main dispersion direction) on the detectors for exposures at different airmasses, we could measure the amount of line shift caused by instrumental flexure to sub-pixel accuracy as a function of row for each detector. Fig. 14 displays one of the typical results in this analysis.

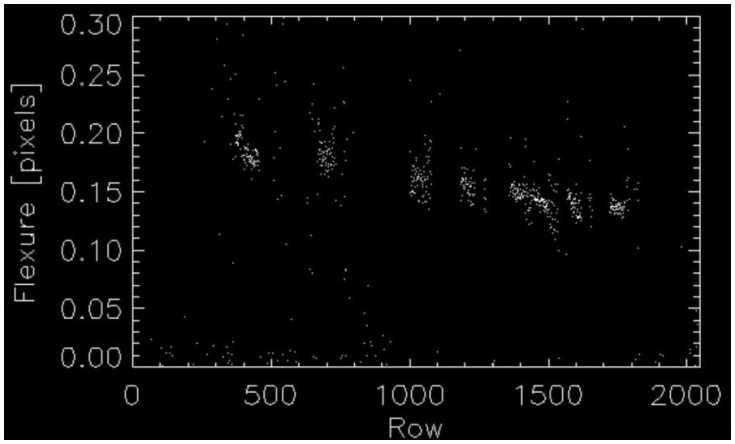

Figure 14 Flexure in the K-band main-dispersion direction in pixels as a function of detector row between airmass 1 (Zenith) and airmass 3. Slit in east-west orientation.

Table 2 summarizes the average flexures measured between airmass 1 and airmass 3 for different orientations of the slit. The K-band images show larger shifts than the H-band echellograms. This result is consistent with the finite-element analysis of the flexure of the optical bench where the greatest deviations with orientation were in the corner of the bench where the K-band camera resides. For the telescope motion along the meridian, north-south slit orientations showed more of flexure than measurements with the slit oriented east-west, a result which is consistent with the structural analyses of collimating mirrors and dichroic mount (Section 2.2). In a real observing situation, where motion is not purely along the meridian, the slit orientation with respect to the changes in the gravity vector will be a combination of the east-west and north-south cases in the test measurements. The average flexure for K band is about 0.4 pixels and this will produce at maximum a shift of 0.1 pixels in the spectral direction during a one-hour exposure. Such a shift would cause an 0.2 km/s RV change if contemporaneous calibration is not applied.

Table 2. Instrumental flexure measured between airmass 1 and airmass 3 in pixels.

Slit orientation	H band [pix]	K band [pix]
East-west	0.01±0.04	0.16±0.04
North-south	0.08±0.02	0.65±0.02

5. CONCLUSION

The IGRINS hardware fabrication and parts assembly for the optical and mechanical components were finished by the end of 2013. We confirmed that IGRINS met its intended design goals through the recent two commissioning runs at the McDonald Observatory 2.7 m Harlan J Smith telescope. During those observations, we debugged the system hardware and software, measured the instrument performance and provided a sample dataset for tests of the data reduction software and for facilitating plans of future astronomical observing programs.

The measured performance of the spectral resolving power turned out to be slightly higher than the designed value of 40,000. That is simply because that we used slightly thinner width of the slit than the originally designed. The measured stellar continuum signal-to-noise ratio resulted in to be more than 80 % of the ETC predicted value, on average, although those commissioning data were not taken in the best optimized instrument conditions. The expected instrumental flexure causes at maximum 0.01 pixels for H-band and 0.1 pixels K-band spectral line shift in one-hour continuous exposure, which is corresponding to 20 m/s and 200 m/s RV measurement uncertainties.

ACKNOWLEDGEMENTS

This work was supported in part by the US National Science Foundation through MRI grant AST-1229522.

REFERENCES

[1] Dekker, H., "An immersion grating for an astronomical spectrograph," in Instrumentation for Ground-Based Optical Astronomy, L. B. Robinson, ed. (Springer-Verlag, Berlin), 183-188 (1988).
[2] Wiedemann, G. and Jennings, D. E., "Immersion grating for infrared astronomy," Appl. Opt. 32, 1176-1178 (1993).
[3] Jaffe, D. T., Keller, L. D., Ershov, O. A., "Micromachined silicon diffraction gratings for infrared spectroscopy," Proc. SPIE 3354, 201-212 (1998).
[4] Marsh, J. P., Mar, D. J., Jaffe, D. T., "Production and evaluation of silicon immersion gratings for infrared astronomy," Appl. Opt. 46, 3400-3416 (2007).
[5] Gully-Santiago, M., Wang, W., Deen, C., and Jaffe, D. T., "Near-infrared metrology of high-performance silicon immersion gratings," Proc. SPIE 8450 (2012).
[6] Wang, W., Gully-Santiago, M., Deen, C., Mar, D. J., Jaffe, D. T., "Manufacturing of silicon immersion gratings for infrared spectrometers," Proc. SPIE 7739 (2010).
[7] Yuk, I. S. et al., "Preliminary design of IGRINS (Immersion GRating INfrared Spectrograph)," Proc. SPIE 7735 (2010).
[8] Barnes, S., "IGRINS optical design report," KASI-UT IGRINS Project Team, 13 (2009).
[9] Jaffe, D. T. et al., "GMTNIRS (Giant Magellan telescope near-infrared spectrograph): optimizing the design for maximum science productivity and minimum risk," Proc. SPIE 9147 (2014).
[10] Kanneganti, S. et al., "FanCam—a near-infrared camera for the Fan Mountain Observatory," PASP 121, 885-896 (2009).
[11] Park, C., Ph.D. Dissertation, "Near-infrared studies of embedded star clusters," University of Virginia, 48 (2010)
[12] Oh, J. S. et al., "Detector mount design for IGRINS," JASS 32(2), 177 (2014).
[13] Rukdee, S. et al., "IGRINS mirror mount design for three off-axis collimators and one slit-viewer fold mirror," JASS 29(2), 233 (2012).
[14] Jeong, U. et al., "Characterization and optimization for detector systems of IGRINS," Proc. SPIE 9154 (2014)
[15] Sim, C. K. et al., "Comprehensive data reduction package for the Immersion GRating INfrared Spectrograph: IGRINS," Advances in Space Research, 53, 1647 (2014).